RSC Advances

ROYAL SOCIETY OF CHEMISTRY

www.rsc.org/advances

Journal Name

RSCPublishing

COMMUNICATION

Palladium modified magnetic mesoporous carbon derived from metal–organic frameworks as a highly efficient and recyclable catalyst for hydrogenation of nitroarenes

Cite this: DOI: 10.1039/xoxxoooooox

Received ooth January 2012,
Accepted ooth January 2012

DOI: 10.1039/xoxxoooooox

www.rsc.org/

Zhengping Dong*, Kun Liang, Chunxu Dong, Xinlin Li, Xuanduong Le, Jiantai Ma*

We present a facile route for the fabrication of palladium modified magnetic nanoparticles (Fe@Pd NPs) embedded in mesoporous carbon (MC), derived from metal–organic frameworks, to produce the Fe@Pd-MC nanocatalyst. The Fe@Pd-MC nanocatalyst exhibited excellent catalytic activity toward the hydrogenation of nitroarenes as well as the easy recovery and reusability.

Introduction

In the recent years, palladium nanoparticles (Pd NPs) have received significant attention because of their remarkable catalytic performances in hydrogenation, C–C coupling, oxidation, and hydrodechlorination reactions.[1-7] They offer high selectivity, efficient catalytic performance, and high conversion. However, agglomeration of the initially well-dispersed Pd NPs throughout the catalytic runs in the reaction solution, is still a drawback in its catalytic applications.[8, 9] Moreover, most Pd NPs catalyzed reactions occur only on the surface of the Pd NPs and a large fraction of atoms in the core remain catalytically inactive, thus should be replaced by other non-noble metals due to the high cost and scarcity of the noble metal resources. To overcome the above mentioned problems and facilitate the recovery of the catalyst, core–shell Pd NPs with non-noble metal core were dispersed onto supporting matrices such as graphene and silica to fabricate heterogeneous Pd catalysts.[7, 10] Therefore, it is highly desirable to design Pd based catalysts with low Pd loading, easy separation property, and high catalytic activity for organic catalytic reactions.

Recently, metal–organic frameworks (MOFs) as a novel class of nanoporous crystalline materials fabricated from transition-metal clusters as nodes and organic ligands as struts have been demonstrated as promising starting materials for the synthesis of mesoporous carbon materials (MC).[11-16] In particular, the transition-metal NPs such as iron (Fe), cobalt (Co), and nickel (Ni) derived from MOFs embedded in MC, can not only act as catalytic active centers, but also reduce the noble metal ions and act as the core to reduce the consumption of the noble metal. Furthermore, the Fe, Co, and Ni NPs also exhibit magnetic property; therefore, introduction of magnetically responsive substance to the catalyst system could endow the magnetic properties to the prepared catalysts, which allows for the easy and efficient recovery of the catalyst from the reaction mixture by using a magnetic field.[13, 17] Extensive research efforts have been devoted to the development of the transition-metal NPs embedded in MC. Thus, a facile and straightforward separation method of noble metal NPs was accomplished either by immobilizing them on the surface of modified magnetic NPs or by supporting them on magnetically responsive materials embedded in MC frameworks. Thus, use of the magnetic MC materials derived from MOFs as support to prepare noble metal based catalysts is extremely meaningful and highly significant.

As important industrial raw materials, substituted anilines are valuable chemicals for the synthesis of various dyes, pharmaceuticals, pigments, and polymers that serve as industrially important organic intermediates for producing pharmaceuticals, dyes stuffs, and functional polymers.[18-20] Till date, aromatic amines are mainly produced by chemoselective hydrogenation of the corresponding nitroarenes over metallic catalysts including noble metals such as platinum (Pt), Pd, ruthenium (Ru), and rhodium (Rh) based catalysts.[19, 21-24] Obviously, Pd NPs based heterogeneous catalysts have excellent catalytic activities and play a very important role in the hydrogenation of nitroarenes due to enhanced fraction of catalytic Pd surface atoms.[25-28] Further, the use of support materials is an extremely significant concept to obtain stable and uniformly distributed Pd NPs without any agglomeration.

Based on the aforementioned considerations, herein, we present a facile route for the fabrication of Fe@Pd NPs embedded in MC, derived from MOFs, to produce the Fe@Pd-MC nanocatalyst. The catalyst support Fe-MC was first prepared through the pyrolysis process during the carbonization of the Fe-MIL-88A under nitrogen and reducing atmosphere, then the Pd^{2+} was reduced by the metallic Fe NPs without adding any reducing agent, and the metallic Pd so-obtained completely covered the exposed surface of Fe NPs with low loading of 0.61 wt%, leading to the formation of Fe@Pd-MC nanocatalyst. The Fe@Pd-MC nanocatalyst exhibited excellent catalytic activity toward the hydrogenation of nitroarenes as well as the easy recovery and reusability property, probably due to the highly dispersed Fe@Pd NPs embedded in MC mesopores. The process reported herein, therefore, inspires the chemists and allows them to design and prepare catalyst materials derived from MOFs with lower noble metal loading and easy magnetic recovery.

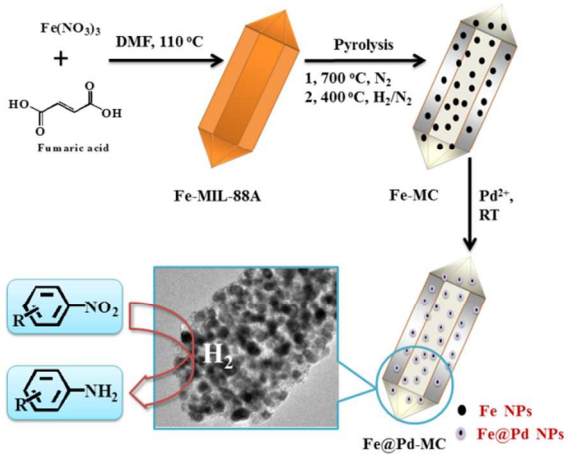

Scheme 1. Preparation of Fe@Pd-MC nanocatalyst.

Experimental

Materials

Fumaric acid, $Fe(NO_3)_3 \cdot 9H_2O$, *N*,*N*-dimethylformamide (DMF), Palladium chloride ($PdCl_2$) and Sodium borohydride ($NaBH_4$) were purchased from Shanghai Chemical Reagent Co., Ltd. All the nitroarenes were also supplied by Shanghai Chemical Reagent Co., Ltd. All other chemicals were of reagent grade purchased from Tianjin Guangfu Chemical Company and used as supplied.

Synthesis of Fe@Pd-MC nanocatalyst

The magnetic mesoporous material was derived from Fe-MIL-88A. First, Fe-MIL-88A was prepared according to the reported solvothermal method.[29] Typically, Fumaric acid (1.68 g, 14.4 mmol) and $Fe(NO_3)_3 \cdot 9H_2O$ (6.4 g, 16 mmol) were dissolved in DMF (300 mL). The resulting mixture was then heated to 110 °C and allowed to stand for 1 h. The resulting Fe-MIL-88A was obtained by successively washing with DMF and methanol via centrifugation redispersion cycles. Second, the dried Fe-MIL-88A (2 g) was calcined up to 700 °C under a nitrogen atmosphere at a heating rate of 2.5 °C min^{-1} in a tube furnace and held at 700 °C for 1 h. After cooling down to 400 °C, H_2 was passed through the tube furnace (H_2/N_2 = 1/3, V/V), and the calcination temperature was maintained at 400 °C for 2 h to thoroughly reduce the iron oxide to metallic Fe NPs. After cooling to room temperature, Fe-MC material was obtained. Third, under inert atmosphere, the Fe-MC material (1 g) was rapidly added into the Pd^{2+} solution (100 mL, [Pd^{2+}] = 1 mg mL^{-1}), and then ultrasonicated for 30 min to reduce Pd^{2+} by Fe. The metallic Pd so-obtained coated the exposed surface of the Fe NPs (Fe@Pd NPs). Finally, the Fe@Pd-MC nanocatalyst was separated by an external magnetic force, thoroughly washed with water (H_2O) and ethanol (EtOH), and dried over night in an oven at room temperature.

General procedure for the hydrogenation of nitroarenes

In a typical procedure, nitroarenes (0.5 mmol) were dissolved in EtOH (5 mL) with Fe@Pd-MC nanocatalyst (5 mg) under an atmosphere of H_2 (rubber balloon) at 20 °C. The reaction was allowed to occur for 1 h, subsequently, the catalyst was separated by an external magnetic force, and the conversion and selectivity of the reaction was estimated by gas chromatography–mass spectroscopy (GC–MS). The separated catalyst was washed several times with EtOH and dried at room temperature for the next catalytic run.

Characterization

Transmission electron microscopy (TEM, Tecnai G^2 F^{30}), scanning electron microscopy (SEM, JSM-6701F) and N_2 adsorption–desorption (ASAP 2010, USA) were used to characterize the morphology of the samples. X-ray diffraction (XRD) measurements were performed on a Rigaku D/max-2400 diffractometer using Cu-Kα radiation as the X-ray source in the 2θ range of 20–80°. X-ray photoelectron spectroscopy (XPS, Perkin-Elmer PHI-5702) was employed to analyze the electronic states of the surface of the samples, and the values of binding energy were calibrated by using C1s = 284.6 eV as a reference. Magnetic measurements on Fe-MC and Fe@Pd-MC nanocatalysts were investigated by a quantum design vibrating sample magnetometer (VSM) at room temperature in an applied magnetic field sweeping from −10 to 10 kOe. The inductively coupled plasma atomic emission spectroscopy (ICP–AES) was used to measure the Pd content of the Fe@Pd-MC nanocatalyst. The conversion and selectivity of the reaction was estimated by GC–MS (Agilent 5977E).

Results and discussion

Characterization of the Catalysts

Scheme 1 shows the schematic representation of the preparation of iron(III) dicarboxylate MOFs of the MIL-88 structure type (Fe-MIL-88A). $Fe(NO_3)_3$ and fumaric acid were employed as the starting reagents and the MOF material, namely, Fe-MIL-88A was prepared according to the reported solvothermal method.[29] Then, under nitrogen and reducing atmosphere, the Fe-MIL-88A was converted to Fe-MC magnetic composite which has metalic Fe NPs embedded in the MC framework. Finally, as the Fe NPs was the only reducing agent that can reduce Pd^{2+} in the following procedure, Pd^{2+} was reduced by Fe NPs and coated on the exposed surface of Fe NPs, thus resulting in the formation of Fe@Pd-MC nanocatalyst.

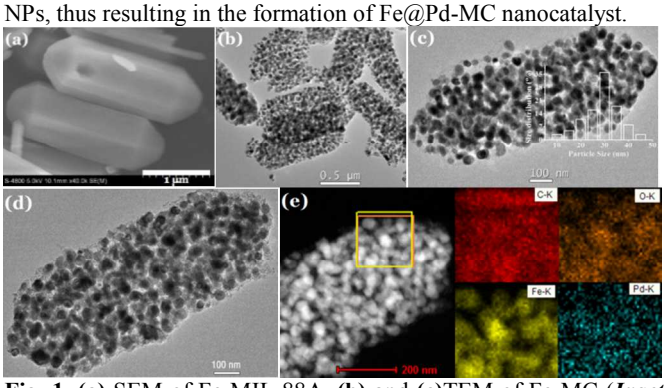

Fig. 1. (a) SEM of Fe-MIL-88A, **(b)** and **(c)**TEM of Fe-MC (***Inset***, size distribution of Fe NPs), **(d)** TEM of Fe@Pd-MC, **(e)** HAADF-STEM image of Fe@Pd-MC, C mapping image (C-K), O mapping image (O-K), Fe mapping image (Fe-K), and Pd mapping image (Pd-K).

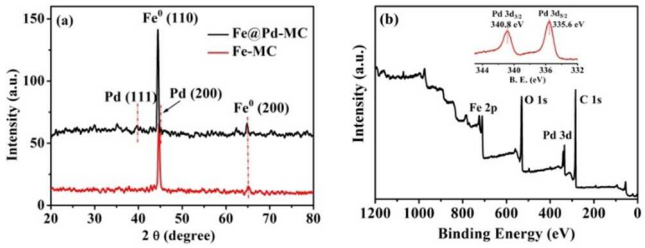

Fig. 2. (a) XRD patterns of Fe-MC and Fe@Pd-MC, **(b)** XPS spectra of Fe@Pd-MC nanocatalyst.

Fig. 1 shows the SEM and TEM images exhibiting the morphology of the samples. The SEM image shows that the Fe-MIL-88A exhibits spindle-like morphology with uniform diameter of about 400 nm and length of about 2 μm (Fig. 1a). In the TEM images of Fe-MC (Figs. 1b and c), the spindle-like morphology was unchanged even after the completion of the pyrolysis process; however, the size seems to be decreased. The pyrolysis and reduction processes led to the conversion of the Fe coordination complexes into Fe NPs, with an average particle size of 30 nm (*Fig. 1c, inset*), embedded in the MC framework. Fe@Pd-MC nanocatalyst was prepared by the reduction of Pd^{2+} by Fe NPs, and then the exposed surface of Fe NPs was coated with metallic Pd. Fig. 1d shows that the morphology of Fe@Pd-MC nanocatalyst still preserves the original form of Fe-MIL-88A and Fe-MC composite. Furthermore, the high-angle annular dark-field scanning transmission electron microscopy (HAADF-STEM) image (Fig. 1e) confirms the detailed elemental distribution of the nanocatalyst. The elemental analysis of the selected-area in the grayscale mapping image clearly indicates that the Fe@Pd-MC nanocatalyst support is mainly composed of carbon element. The catalytic activity center, Pd (green) is well dispersed on the Fe NPs (yellow) and embedded in the MC framework.

Further, the crystallographic structures of the samples were determined by XRD. Fig. 2a exhibits the XRD pattern of Fe-MC displaying two peaks at 2θ = 44.8°, 65.4° which are in well agreement with the characteristic peaks of (110) and (200) planes of metallic α-Fe (JCPDS No. 65-4899), respectively. The size of the Fe NPs calculated by the Scherrer formula is about 30 nm, which is almost similar to that obtained by the TEM observation. Compared to the XRD pattern of Fe-MC, Fe@Pd-MC shows two characteristic diffraction peaks at 2θ = 39.9 and 45.2° corresponding to Pd (111) and Pd (200) of Pd (JCPDS 46-1043), respectively,[2, 30] revealing that the Pd^{2+} was successfully reduced to metallic Pd and grafted on the surface of Fe NPs. Moreover, the weak peaks of Pd in the XRD pattern also indicate its low content in Fe@Pd-MC. The weight percentage of Pd loading obtained from ICP–AES measurement is about 0.61 wt%. The state of the Pd in Fe@Pd-MC is determined by XPS. Fig. 2b clearly shows the characteristic peaks of metallic Pd, and the peaks at 335.6 and 340.8 eV are respectively assigned to Pd $3d_{5/2}$ and Pd $3d_{3/2}$, revealing that Pd^{2+} is not existed in the framework of Fe-MC, and the adsorbed Pd^{2+} has been completely reduced to metallic Pd.

The N_2 adsorption–desorption isotherms and pore size distribution curves of the Fe-MC and Fe@Pd-MC composites are shown in Fig. 3a. The isotherms with steep increases at relatively high pressure ($P/P_0 > 0.5$) is a typical type-IV behavior, indicating the existence of large amount of mesopores, resulting from the pyrolysis process during the carbonization of the Fe-MIL-88A.[16, 31] The Brunauer–Emmett–Teller specific surface area of Fe-MC is 97.6 $m^2\ g^{-1}$; however, the surface area of Fe@Pd-MC is only 86.3 $m^2\ g^{-1}$. Fig. 3a *inset* clearly shows that the main pore size distributions of Fe-MC and Fe@Pd-MC are 5–20 and 5–18 nm, respectively. The slightly decrease both in the specific surface area and pore size probably due to the exposed surface of the Fe NPs was coated with Pd atoms which have larger diameter than Fe atoms. The magnetic properties of the samples were measured in fields between ±10 kOe at room temperature. Both the samples exhibit ferromagnetic properties with saturated magnetization (Ms) and coercivity (Hc) values of 136 emu g^{-1} and 450 Oe; and 120 emu g^{-1} and 334 Oe, respectively for Fe-MC and Fe@Pd-MC (Fig. 3b). Therefore, Fe@Pd-MC nanocatalyst could be efficiently separated from the reaction mixture by an external magnetic force and reused (Fig. 3b, *inset*) in the subsequent catalytic runs.

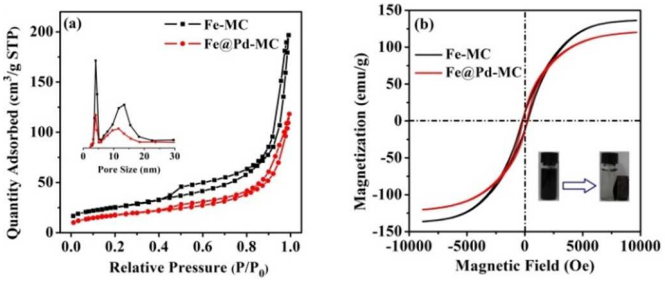

Fig. 3. (a) N_2 sorption isotherms of Fe-MC and Fe@Pd-MC (***Inset*** is the pore size distributions of Fe-MC and Fe@Pd-MC). **(b)** Room temperature magnetization curves of Fe-MC and Fe@Pd-MC.

Table 1. Solvent screening of the Fe@Pd-MC nanocatalyst catalyzed hydrogenation of nitrobenzene.

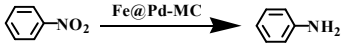

Entry	Solvent	T (°C)	Time (h)	Yield (%)
1	EtOH	20	1	>99
2	MeOH	20	1	98.1
3	ethyl acetate	20	1	98.9
4	THF	20	1	48.8
5	DMF	20	1	24.7
6	cyclohexane	20	1	94.2
7	H_2O	20	1	73.9
8	toluene	20	1	91.8

Reaction conditions: nitrobenzene (0.5 mmol), Fe@Pd-MC nanocatalyst (5 mg, 0.06 mol% Pd relative to nitrobenzene), H_2 (1 atm), solvent (5 mL), reaction time (1 h).

Hydrogenation of nitroarenes

Scheme 1 demonstrates that the prepared Fe@Pd-MC nancatalyst is utilized to catalyze the hydrogenation of nitroarenes. The catalytic hydrogenation of nitroarenes commenced with a solvent screening, using nitrobenzene as the model substrate (Table 1). In a typical reaction, nitrobenzene (0.5 mmol) and Fe@Pd-MC nanocatalyst (5 mg) were suspended in 5 mL of solvent and vigorously stirred under 1 atm of H_2 at 20 °C. The values listed in Table 1 indicated that when the hydrogenation was performed in EtOH as the reaction solvent, more than 99% conversion to the product occurred. Thus, EtOH was selected as the optimized solvent for the hydrogenation of various nitroarenes under atmospheric H_2 at room temperature in 1 h.

Based on the optimized reaction conditions, we then extended the Fe@Pd-MC nanocatalyst to various nitroarenes to examine the generality of the reaction (Table 2). In all cases, the desired aromatic amines were obtained in excellent yields of over 94%. The electronic features of the nitroarenes almost did not affect the reaction yield. Importantly, several reducible groups, like OH, CN, $COCH_3$, and COOH remained totally unaffected under the reaction conditions (Table 2, entries 3–9). Notably, the hydrogenation reactions of nitroaniline also occurred selectively to give the corresponding diphenylamines in high yields exceeding 96% (Table 2, entries 10–12), and the hydrogenation of 2,4-dinitroaniline produced high yield (98.3%, Table 2, entry 13) of the product. The efficient

hydrogenation of nitroarenes was probably due to the Fe@Pd-MC nanocatalyst with large pore size that could significantly enhance the mass transfer, thus allowing for the easy and efficient contact between the reactants and the active sites (Fe@Pd NPs), leading to rapid commencement and completion of the reaction. The mechanism of the hydrogenation of nitroarenes was as follows: Initially, H_2 molecule was dissociated on the metallic Pd surface to provide dissociative hydrogen species. Nitro compounds are not directly adsorbed on the surface of the catalyst; however may have an interaction with the dissociative hydrogen species. The reduction occurred in steps and initially the nitro-compound was reduced to the nitroso-compound which was further reduced to the hydroxyamino compound. Finally, hydroxyl amine was reduced to aniline.[20, 32, 33]

Table 2. Hydrogenation of various nitroarenes using Fe@Pd-MC nanocatalyst.

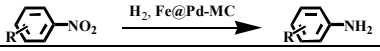

Entry	Substrate	Product	Yield (%)
1			99.6
2			95.5
3	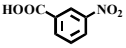	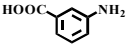	94.2
4	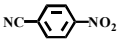	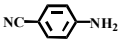	98.8
5	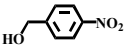	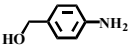	97.2
6	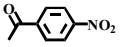	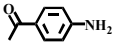	99.1
7	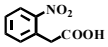	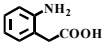	98.9
8			98.9
9	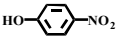	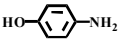	96.2
10			96.6
11		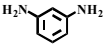	98.2
12		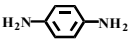	94.4
13	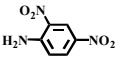	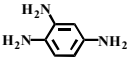	98.3

Reaction conditions: substrate (0.5 mmol), Fe@Pd-MC nanocatalyst (5 mg, 0.06 mol% Pd relative to substrate), H_2 (1 atm), solvent (5 mL), reaction time (1 h). Yield was determined by GC-MS.

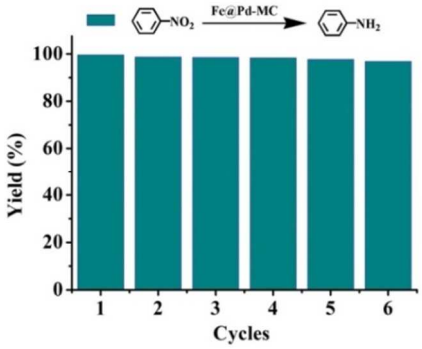

Fig. 4. The reusability of the Fe@Pd-MC nanocatalyst for hydrogenation of nitrobenzene.

Recycling and reusability of the catalyst are definitely important in the heterogeneous catalytic reactions. Therefore, we investigated the recyclability of the Fe@Pd-MC nanocatalyst for chemoselective hydrogenation reaction using nitrobenzene as a model substrate. The Fe@Pd-MC nanocatalyst could be efficiently separated from the reaction mixture by an external magnetic force owing to its superparamagnetic property; and the recovered catalyst was repeatedly washed with EtOH and dried at room temperature for the next catalytic run. Fig. 4 shows that the catalyst Fe@Pd-MC does not exhibit any change in its activity (conversion and selectivity), and the loss in the yields of aromatic anilines are not observed even after six successive runs. The amount of Pd present in the catalyst after six runs is about 0.59 wt% which is almost similar to the amount present in the fresh catalyst (estimated by ICP–AES), thus confirming the stability of the catalyst.

Conclusions

Fe@Pd-MC nanocatalyst with low Pd loading was prepared by embedding Fe@Pd NPs in the MC, derived from MOFs, and used for the catalytic hydrogenation of various nitroarenes in the presence of atmospheric H_2 at room temperature. The nanocatalyst exhibited excellent catalytic activity in the hydrogenation of nitroarenes and also could be easily recycled and reused, attributed to its superparamagnetic property. This study is believed to be extremely beneficial to design and prepare catalyst materials derived from MOFs, with lower noble metal loading and efficient and convenient magnetic recovery.

Notes and references

College of Chemistry and Chemical Engineering, Gansu Provincial Engineering Laboratory for Chemical Catalysis, Lanzhou University, Lanzhou 730000, PR China.
∗ Corresponding authors. Tel.: +86 0931 8912577; fax: +86 0931 8912582. E–mail addresses: dongzhp@lzu.edu.cn (Zhengping Dong), majiantai@lzu.edu.cn (Jiantai Ma).

1. P. Zhang, T. B. Wu, M. Q. Hou, J. Ma, H. Z. Liu, T. Jiang, W. T. Wang, C. Y. Wu and B. X. Han, *Chemcatchem*, 2014, 6, 3323-3327.
2. J. Sun, Y. Fu, G. He, X. Sun and X. Wang, *Appl. Catal. B: Environ.*, 2015, 165, 661-667.
3. A. J. R. Hensley, Y. Wang and J.-S. McEwen, *ACS Catal.*, 2014, 523-536.
4. C. B. Molina, A. H. Pizarro, J. A. Casas and J. J. Rodriguez, *Appl. Catal. B: Environ.*, 2014, 148-149, 330-338.
5. L. Shang, T. Bian, B. Zhang, D. Zhang, L.-Z. Wu, C.-H. Tung, Y. Yin and T. Zhang, *Angew. Chem. Int. Edit.*, 2014, 53, 250-254.
6. K. Chung, S. M. Banik, A. G. De Crisci, D. M. Pearson, T. R. Blake, J. V. Olsson, A. J. Ingram, R. N. Zare and R. M. Waymouth, *J. Am. Chem. Soc.*, 2013, 135, 7593-7602.
7. Z. Dong, X. Le, C. Dong, W. Zhang, X. Li and J. Ma, *Appl. Catal. B: Environ.*, 2015, 162, 372-380.
8. M. Gulcan, M. Zahmakiran and S. Özkar, *Appl. Catal. B: Environ.*, 2014, 147, 394-401.
9. Q.-L. Zhu, N. Tsumori and Q. Xu, *Chem Sci*, 2014, 5, 195-199.
10. O. Metin, S. F. Ho, C. Alp, H. Can, M. N. Mankin, M. S. Gultekin, M. Chi and S. Sun, *Nano Research*, 2013, 6, 10-18.
11. Y. Yang, Y. Zhang, C. J. Sun, X. Li, W. Zhang, X. Ma, Y. Ren and X. Zhang, *Chemcatchem*, 2014, 6, 3084-3090.
12. A. Banerjee, R. Gokhale, S. Bhatnagar, J. Jog, M. Bhardwaj, B. Lefez, B. Hannoyer and S. Ogale, *J. Mater. Chem.*, 2012, 22, 19694-19699.
13. A. J. Amali, J.-K. Sun and Q. Xu, *Chem. Commun.*, 2014, 50, 1519-1522.
14. N. L. Torad, M. Hu, S. Ishihara, H. Sukegawa, A. A. Belik, M. Imura, K. Ariga, Y. Sakka and Y. Yamauchi, *Small*, 2014, 10, 2096-2107.

15. J. Yang, C. Zheng, P. Xiong, Y. Li and M. Wei, *J. Mater. Chem. A*, 2014, 2, 19005-19010.
16. F. Zou, X. Hu, Z. Li, L. Qie, C. Hu, R. Zeng, Y. Jiang and Y. Huang, *Adv Mater.*, 2014, 26, 6622-6628.
17. Y. N. Wu, M. Zhou, S. Li, Z. Li, J. Li, B. Wu, G. Li, F. Li and X. Guan, *Small*, 2014, 10, 2927-2936.
18. Z. Zhao, H. Yang, Y. Li and X. Guo, *Green. Chem.*, 2014, 16, 1274-1281.
19. O. Verho, K. P. J. Gustafson, A. Nagendiran, C.-W. Tai and J.-E. Bäckvall, *Chemcatchem*, 2014, 6, 3153-3159.
20. D. V. Jawale, E. Gravel, C. Boudet, N. Shah, V. Geertsen, H. Li, I. N. Namboothiri and E. Doris, *Chem. Commun.*, 2015, 51, 1739-1742.
21. P. Tomkins, E. Gebauer-Henke, W. Leitner and T. E. Müller, *ACS Catal.*, 2014, 203-209.
22. M. Xie, F. Zhang, Y. Long and J. Ma, *RSC Adv.*, 2013, 3, 10329-10334.
23. Q. Sun, C.-Z. Guo, G.-H. Wang, W.-C. Li, H.-J. Bongard and A.-H. Lu, *Chem. Eur. J.*, 2013, 19, 6217-6220.
24. H. Wei, X. Liu, A. Wang, L. Zhang, B. Qiao, X. Yang, Y. Huang, S. Miao, J. Liu and T. Zhang, *Nat. Commun.*, 2014, 5, 5634.
25. H. Goksu, S. F. Ho, O. Metin, K. Korkmaz, A. M. Garcia, M. S. Gultekin and S. Sun, *ACS Catal.*, 2014, 4, 1777-1782.
26. Z. Li, J. Li, J. Liu, Z. Zhao, C. Xia and F. Li, *Chemcatchem*, 2014, 6, 1333-1339.
27. H. Zhao, Y. Wang and R. Wang, *Chem. Commun.*, 2014, 50, 10871-10874.
28. Y.-S. Feng, J.-J. Ma, Y.-M. Kang and H.-J. Xu, *Tetrahedron*, 2014, 70, 6100-6105.
29. C. Serre, F. Millange, S. Surblé and G. Férey, *Angew. Chem. Int. Edit.*, 2004, 43, 6285-6289.
30. X. Le, Z. Dong, X. Li, W. Zhang, M. Le and J. Ma, *Catal. Commun.*, 2015, 59, 21-25.
31. Y. Liu, N. Zhang, L. Jiao, Z. Tao and J. Chen, *Adv. Funct. Mater.*, 2015, 25, 214-220.
32. A. Shukla, R. K. Singha, T. Sasaki and R. Bal, *Green Chem.*, 2015, DOI: 10.1039/c4gc01664e.
33. S. Cai, H. Duan, H. Rong, D. Wang, L. Li, W. He and Y. Li, *ACS Catal.*, 2013, 3, 608-612.